## Title

Phosphorothioate RNA Analysis by NETD Tandem Mass Spectrometry.



## Journal

Molecular & Cellular Proteomics, 23(4)

## Authors

Peters-Clarke, Trenton
Quan, Qiuwen
Anderson, Benton
et al.

## Publication Date

2024-04-01

## DOI

10.1016/j.mcpro.2024.100742

Peer reviewed

# Phosphorothioate RNA Analysis by NETD Tandem Mass Spectrometry


## Authors

Trenton M. Peters-Clarke, Qiuwen Quan, Benton J. Anderson, William M. McGee, Emily Lohr, Alexander S. Hebert, Michael S. Westphall, and Joshua J. Coon

## Correspondence

jcoon@chem.wisc.edu


## In Brief


Therapeutic RNAs are routinely modified during their synthesis to ensure proper drug uptake, stability, and efficacy. Here, we comprehensively analyze phosphorothioate-modified RNA via tandem mass spectrometry. We show that activated ion-negative electron transfer dissociation MS/MS is especially useful, producing diagnostic a- and z-type ions at modification sites. We also present OligoSeq, a C# platform for direct sequence and modification characterization of oligonucleotides. These findings should inform how researchers annotate MS/MS data of partially or fully modified phosphorothioate RNA.


## Graphical Abstract

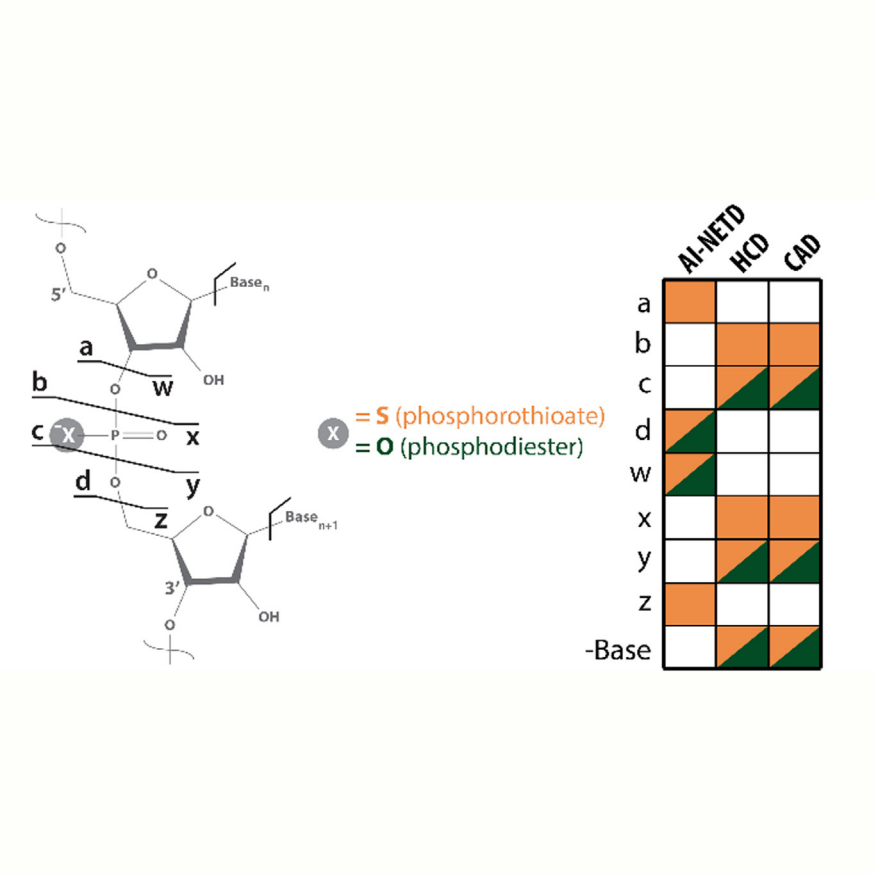


## Highlights

- AI-NETD enables complete sequence coverage of therapeutic RNAs.
- Phosphorothioate modifications influence nucleic acid dissociation.
- AI-NETD generates site-specific a- and z-type ions at phosphorothioate linkages.
- Collisional activation produces b- and x-type ions in phosphorothioate RNAs.


**2024, Mol Cell Proteomics *23*(*4*), 100742**



**https://doi.org/10.1016/j.mcpro.2024.100742**

# Phosphorothioate RNA Analysis by NETD Tandem Mass Spectrometry

Trenton M. Peters-Clarke[1,2], Qiuwen Quan[2], Benton J. Anderson[1,2], William M. McGee[3], Emily Lohr[2], Alexander S. Hebert[2,4], Michael S. Westphall[2,4], and Joshua J. Coon[1,2,4,5,*]

**Therapeutic RNAs are routinely modified during their synthesis to ensure proper drug uptake, stability, and efficacy. Phosphorothioate (PS) RNA, molecules in which one or more backbone phosphates are modified with a sulfur atom in place of standard nonbridging oxygen, is one of the most common modifications because of ease of synthesis and pharmacokinetic benefits. Quality assessment of RNA synthesis, including modification incorporation, is essential for drug selectivity and performance, and the synthetic nature of the PS linkage incorporation often reveals impurities. Here, we present a comprehensive analysis of PS RNA *via* tandem mass spectrometry (MS). We show that activated ion-negative electron transfer dissociation MS/MS is especially useful in diagnosing PS incorporation, producing diagnostic a- and z-type ions at PS linkage sites, beyond the standard d- and w-type ions. Analysis using resonant and beam-type collision-based activation reveals that, overall, more intense sequence ions and base-loss ions result when a PS modification is present. Furthermore, we report increased detection of b- and x-type product ions at sites of PS incorporation, in addition to the standard c- and y-type ions. This work reveals that the gas-phase chemical stability afforded by sulfur alters RNA dissociation and necessitates inclusion of additional product ions for MS/MS of PS RNA.**

## JJC DEDICATION

We are pleased to contribute this manuscript to honor Don Hunt in this special issue of *Molecular & Cellular Proteomics*. I had the good fortune to join Don's laboratory in January 2003 as a postdoctoral student. My project, together with John Syka, was to modify a linear ion trap mass spectrometer to do the ion/ion analog of electron capture dissociation. Don's laboratory was an amazing place, serving as my introduction to shotgun proteomics. During my time, there we were fortunate, and our experiments led to the discovery of ETD. After we had figured out ETD, and before I left Charlottesville for Madison, we ran the reaction in reverse and called the method NETD.

Having just joined the Chemistry Department at the University of Wisconsin, I thought I should have a publication in the *Journal of the American Chemical Society* and suggested to Don that we try reporting the NETD work there. Don did not think we would get in, as most important analytical work does not. In fact, Don actually bet me a quarter that I would not get the manuscript published in the *Journal of the American Chemical Society*. Unfortunately, Don was correct, and it was rejected. No matter, we found a good home for it (1).

Here in Wisconsin, we have continued to develop the technique but mostly for peptide anions. With the increasing importance of RNA therapeutics, and the need to characterize these challenging molecules, we have recently revisited NETD. This work describes our latest efforts, the promise of this method, and serves as a tribute to the impact of Don Hunt on MS and its biomedical application.

Since the discovery over 50 years ago that a short DNA oligonucleotide could site-specifically inhibit viral translation and cell transformation (2, 3), research has uncovered the potential of antisense oligonucleotides for therapeutic intervention (4, 5). Recent success has been driven, in large part, by the integration of chemical modifications to the nucleobase, the ribose or deoxyribose sugar, or within the phosphate backbone. These modifications can introduce steric selectivity, inhibit nuclease activity, and targeted delivery of RNA to tissues of interest. The burgeoning role of diverse modifications in RNA therapeutics demands efficient workflows for comprehensive characterization of therapeutic oligonucleotides.

Avoiding immune recognition and degradation is critical for successful delivery, and various chemical modifications can impart therapeutic properties. 2′-O-methyl and 2-fluoro modifications are used in CRISPR–Cas9 guide RNA (gRNA), siRNA, mRNA therapeutics, and exon-skipping antisense

From the [1]Department of Chemistry, University of Wisconsin-Madison, Madison, Wisconsin, USA; [2]Department of Biomolecular Chemistry, University of Wisconsin-Madison, Madison, Wisconsin, USA; [3]Thermo Fisher Scientific, San Jose, California, USA; [4]National Center for Quantitative Biology of Complex Systems, Madison, Wisconsin, USA; [5]Morgridge Institute for Research, Madison, Wisconsin, USA
*For correspondence: Joshua J. Coon, jcoon@chem.wisc.edu.





https://doi.org/10.1016/j.mcpro.2024.100742

oligonucleotides (4, 5). Conjugation of triantennary GalNAc to siRNA can boost delivery to hepatocytes *in vivo* (6). Incorporation of noncanonical nucleobases such as $N^1$-methylpsuedouridine and 5-methylcytidine to mRNA can confer biological stability and increased protein expression (7–12), including for coronavirus disease 2019 mRNA vaccines produced by Pfizer-BioNTech (BNT162b2 vaccine) and Moderna (mRNA-1273 vaccine) (11, 12). Phosphorothioate (PS) linkages in which a nonbridging oxygen atom of the phosphate is replaced with sulfur (13–15) facilitates cellular uptake and bioavailability *in vivo*, so most therapeutic oligonucleotides contain some degree of PS modification (6, 15–18).The integral nature of these modifications on RNAs necessitates their analysis to obtain a comprehensive characterization of oligonucleotides.

Tandem mass spectrometry (MS/MS) has emerged as a centerpiece technology to address modified oligonucleotide analysis but faces several challenges (19–22). The most common methods are collisional-based activation, including resonant collision-activated dissociation (*i.e.*, ion trap CAD) and beam-type collision-activated dissociation (a.k.a., higher-energy collisional dissociation [HCD]) because of their speed and accessibility (23, 24). However, these methods primarily direct RNA cleavage across numerous channels, yielding complex spectra through the generation of internal fragments and neutral nucleobase loss. Although the formation of these unintended products can be mitigated for CAD by selecting lower charge-state precursors (25–28), it is beneficial to consider alternative methods and their potentials in oligonucleotide characterization.

Over the past 3 decades, several groups have pioneered alternatives to collisions for activation of oligonucleotides. Electron capture dissociation (29–31) and electron transfer dissociation (ETD) (32, 33) are useful ion–ion reactions, though their dependence on oligonucleotide cations is a drawback. Since RNA is amenable to negative mode analysis because of its highly acid nature, it is more suitable for generation of multiply deprotonated anions. Several chemistries amenable to anion activation have been developed, including negative electron transfer dissociation (NETD) (34–41), electron detachment dissociation (42–44), and radical transfer dissociation (45). The development of NETD for the dissociation of nucleic acid anions by McLuckey *et al.* (39) predates development of the positive-mode analog, ETD. The activation of nucleic acids with photons, *via* ultraviolet photodissociation (46, 47), IR multiphoton dissociation (31) or hybrid methods that utilize photons and electrons has proven useful for a range of small and large oligonucleotides (38, 47–52). Because of the challenge of generating comprehensive sequence coverage for larger oligonucleotides, common workflows digest CRISPR gRNA (53, 54), siRNA (55), and mRNA (56, 57) with ribonucleases, in a manner analogous to shotgun proteomics, with the intent to create shorter oligonucleotides more amenable to collision-based activation. The analysis of intact or native oligonucleotides is preferable as it enables analysis of sample purity, modification heterogeneity, and RNA– or DNA–ligand interactions. Indeed, several groups have reported the study of intact oligonucleotides (21, 36, 43, 44, 58–60).

Recently, we introduced a novel implementation of NETD that allowed for activation of anions with fluoranthene cations and synchronous IR photoactivation on a commercially available quadrupole-Orbitrap-linear ion trap hybrid mass spectrometer (38). Activated ion NETD (AI-NETD) has generated comprehensive sequence coverage for methylated RNA up to 7 kDa (38), catalyst-bound DNA hairpins up to 16 kDa (58, 60), and peptide anions (1, 61–65). We were curious how AI-NETD, a softer, nonergodic process (1, 66–68), may perform relative to collision-based methods on intact therapeutic PS RNA sequences. Previous MS studies of oligonucleotides indicate certain modifications may affect MS/MS fragmentation patterns for a limited oligonucleotide sample set, which focused more on sequence coverage outputs. We hypothesized that the fragmentation patterns driven by collisions or electrons may change upon introduction of sulfur atoms to the nucleic acid backbone. To test this hypothesis, we synthesized a library of RNAs with varying degrees of PS incorporation, allowing for each residue's influence to be individually analyzed (Table 1). We reveal that PS RNAs are readily sequenced with up to 100% sequence coverage using AI-NETD and have an altered landscape of fragment ions. An unmodified 20-mer RNA produces d- and w-type ions; however, as PS modifications are introduced, a- and z- type ions are detected in equal proportion, specifically at sites of PS incorporation. We hypothesize that the sulfur influences initial electron transfer and allows for increased gas-phase stability of a- and z-type ions.

As a point of comparison, we analyzed the same PS RNAs with ion trap CAD and beam-type CAD MS/MS experiments. Under these conditions, the unmodified 20-mer features primarily c- and y-type ion production. Upon incorporation of PS modifications, a substantial increase in b- and x-type ion production is observed specifically at sites of PS incorporation for both CAD and HCD. Furthermore, we find that beam-type CAD produces more intense fragment ions, *via* both phosphodiester backbone fragmentation and *via* nucleobase loss, when a PS modification is present at that residue. We also present OligoSeq, a C# software platform for the direct sequence and modification characterization of oligonucleotides from MS data. Overall, we believe these findings should inform how researchers annotate MS/MS data of partially or fully modified PS RNA. Accurately annotating or searching spectra against a database relies on knowledge of relevant product ions, allowing for more robust analysis by reducing search times and increasing confidence in spectral matching.

TABLE 1
*Summary of the RNA sequences used in this study*

| Name | Sequence | Mass (Da) |
|---|---|---|
| Unmodified RNA | 5′-U A C A G C A U C G G C C U G G A C AU-3′ | 6362.89 |
| 9ps RNA | 5′-U A*C A*G C*A U*C G*G C*C U*G G*A C*AU-3′ | 6507.48 |
| 10ps RNA | 5′-U A*C A*G C*A U*C*G*G C*C U*G G*A C*AU-3′ | 6523.55 |
| 11ps RNA | 5′-U A*C A*G C*A U*C*G*G*C*C U*G G*A C*AU-3′ | 6539.61 |
| 12ps RNA | 5′-U A*C A*G C*A*U*C*G*G*C*C U*G G*A C*AU-3′ | 6555.68 |
| 13ps RNA | 5′-U A*C A*G C*A*U*C*G*G*C*C*U*G G*A C*AU-3′ | 6571.74 |
| 14ps RNA | 5′-U A*C A*G*C*A*U*C*G*G*C*C*U*G G*A C*AU-3′ | 6587.81 |
| 15ps RNA | 5′-U A*C A*G*C*A*U*C*G*G*C*C*U*G*G*A C*AU-3′ | 6603.88 |
| 16ps RNA | 5′-U A*C*A*G*C*A*U*C*G*G*C*C*U*G*G*A C*AU-3′ | 6619.94 |
| 17ps RNA | 5′-U A*C*A*G*C*A*U*C*G*G*C*C*U*G*G*A*C*AU-3′ | 6636.01 |
| 18ps RNA | 5′-U*A*C*A*G*C*A*U*C*G*G*C*C*U*G*G*A*C*AU-3′ | 6652.07 |
| Fullps RNA | 5′-U*A*C*A*G*C*A*U*C*G*G*C*C*U*G*G*A*C*A*U-3′ | 6668.14 |

The full sequence for the variably modified 20-mer RNAs is shown as well as theoretical monoisotopic masses. *Asterisks* (*) denote phosphorothioate linkages.

## EXPERIMENTAL PROCEDURES

### *Materials*

All unmodified and PS-modified RNAs were obtained from Integrated DNA Technologies on the 1.0 μmol scale and used without further purification. All oligonucleotides contained 3′- and 5′-terminal hydroxyl groups. See Table 1 for a summary of ribooligonucleotides used in this study. Oligonucleotides all have the same nucleotide sequence, corresponding to the first 20 nt of CRISPR gRNA, with varied PS modification incorporation. Oligonucleotide single-strand concentrations were determined spectrophotometrically by Beer's law using the extinction coefficients provided by the manufacturer. For electrospray MS analysis, solutions were diluted to 5 pmol/μl of oligonucleotide by preparing in 30:70 acetonitrile:$H_2O$ with 15 mM ammonium acetate. Acetonitrile (HPLC grade), $H_2O$ (HPLC grade), and ammonium acetate (LC–MS grade) were obtained from Sigma–Aldrich.

### *MS*

All MS and MS/MS experiments were performed on a quadrupole-Orbitrap-quadrupole linear ion trap (q-OT-LTQ) hybrid mass spectrometer system (Orbitrap Fusion Lumos; Thermo Fisher Scientific), which was modified to perform NETD. Furthermore, the mass spectrometer was retrofitted to include a Firestar ti60 Synrad 60 W $CO_2$ continuous wave IR laser (10.6 μm) to allow for excitation of precursor ions within the quadrupole linear ion trap (69, 70). The IR photon beam waist is calculated to be approximately 2.0 mm within the center section of the high-pressure linear ion trap. RNA samples were directly infused at a flow rate of 3 μl/min using a Hamilton GasTight Valco syringe and a Chemyx Fusion 101 syringe pump. RNA anions were generated *via* electrospray ionization in the negative mode with an electrospray voltage of −2.8 kV relative to ground and a transfer tube temperature of 275 °C. The ion funnel RF was held at 60%, and the source nitrogen sheath and auxiliary gas were held at 10 and 5 arbitrary units, respectively, to aid in desolvation.

For LC–MS/MS analyses, oligonucleotides were separated using hydrophilic interaction chromatography over a 30 min active gradient on a Waters BEH Amide 1.7 μm (2.1 × 150 mm) column using a Dionex Ultimate 3000 LC. Mobile phase A was 10 mM ammonium acetate with 0.025% acetic acid in 70:30 acetonitrile:water. Mobile phase B (MPB) was 10 mM ammonium acetate with 0.025% acetic acid in 90:10 isopropanol:acetonitrile. Using a flow rate of 0.4 ml/min, the gradient ramped from 20 to 30% MPB from 1 to 4 min, 30 to 45% MPB from 4 to 30 min, 45 to 85% MPB from 30 to 31 min, held at 85% MPB from 31 to 33 min, reduced to 10% MPB from 33 to 34 min, and held at 10% MPB until 45 min. The LC was connected on-line with a Q-Exactive HF mass spectrometer. MS1 parameters included 70,000 resolving power at *m/z* 200 with an automatic gain control target of 3E6, maximum injection time of 100 ms, and *m/z* range of 500 to 3000 with data collected in profile mode. Data-dependent MS2 scans were collected at 70,000 resolving power at *m/z* 200 with an automatic gain control target of 1E5, maximum injection time of 300 ms, isolation width of 4.0 Th, *m/z* range of 200 to 2000, and stepped collision energies of 15, 20, and 25 normalized collision energy.

When performing electron-based dissociation with NETD and AI-NETD, precursor anions were selected by in the quadrupole with a 1.2 Th isolation window and were accumulated in the middle section of the high-pressure linear ion trap. Next, reagent fluoranthene radical cations (*m/z* 202.08) were generated in the front-end chemical ionization source and routed to the front section of the high-pressure linear ion trap (38). Removal of the direct current potential well and application of a secondary RF voltage to the end lenses allowed for charge-sign independent axial trapping and mixing of RNA anions with reagent cations. The NETD reaction was terminated by axial ejection of reagent cation species and subsequent routing of negatively charged fragment ions and unreacted precursor to the Orbitrap for collection of a high-resolution MS/MS spectrum. MS/MS spectra were collected at 120,000 resolving power at *m/z* 200. Data were collected in profile mode, and for increased statistics, MS/MS spectra are the average of 25 individual scans, with averaging performed in the vendor's postacquisition software (XCalibur Qual Browser, version 2.2). No microscans were performed. During AI-NETD experiments, the 60 W continuous wave $CO_2$ laser irradiated the center section of the trapping volume for the duration of the ion–ion reaction only. The IR laser power output was controlled externally and varied from 4 W (7% maximal output) to 12 W (20% maximal output).

For collision-based dissociation with resonant CAD and beam-type HCD experiments, several collisional energies and precursor charge states were tested to optimize dissociation efficiency. For resonant CAD, an activation time of 10 ms was used with a *q* value of 0.3 at the precursor *m/z*. Quadrupole isolation and Orbitrap mass analysis was performed with the same parameters as in the NETD experiments described above.

### *Data analysis*

Here, we present OligoSeq, a software platform for the direct sequence and modification characterization of oligonucleotides from

MS data. OligoSeq is based on the design framework of the C# Mass Spectrometry Library (CSMSL, https://github.com/dbaileychess.com/CSMSL) and can handle RNA, DNA, or mixed-base input sequences. Users simply need to enter the .raw file location, oligonucleotide sequence, precursor charge state, and whether the oligonucleotide is an RNA or a DNA. Furthermore, synthetic or post-transcriptional modifications can be easily installed at any location along the sequence. OligoSeq can incorporate modifications to the ribose sugar (*e.g.*, 2′-O-methyl RNA or 2′-O-flouro RNA), modifications to the nitrogenous nucleobase, (*e.g.*, 6-methyladenosine), modifications to the phosphodiester backbone (*e.g.*, PS linkages), or modifications to the 5′ or 3′ termini. Users can also include noncanonical nucleobases, such as wybutosine or 5-methyldeoxycytosine (71). The software was written to incorporate the diverse range of potential modifications referenced in the RNA modification database (72–75).

While directly reading in Thermo XCalibur .raw files, OligoSeq allows for facile extraction of fragment ions and their intensities, with oligonucleotide dissociation nomenclature illustrated in Figure 1. Spectrum-matched base-loss fragments and internal fragments can also be searched. The mass tolerance for matching experimental features to theoretical product ions can be set in either ppm or Daltons. The default mass tolerance is 10 ppm for Orbitrap MS/MS scans and 0.03 Da for ion trap MS/MS scans; however, users can set their preferred mass tolerance for fragment matching. OligoSeq generates annotated data in tabular format, enabling the rapid interpretation of MS/MS spectra for ion statistics, sequence coverage, and modification localization. For the present study, all fragment ion matches were made within a 10 ppm tolerance of the theoretical mass. Because of the slight palindromic nature of the nucleic acids used and product types available, some indistinguishable overlaps in coverage may occur. OligoSeq source code is freely available at https://github.com/coongroup/Transcriptomics for custom implementations. Python code to reproduce data analysis is available at https://github.com/benton-anderson/sulfur_rna.

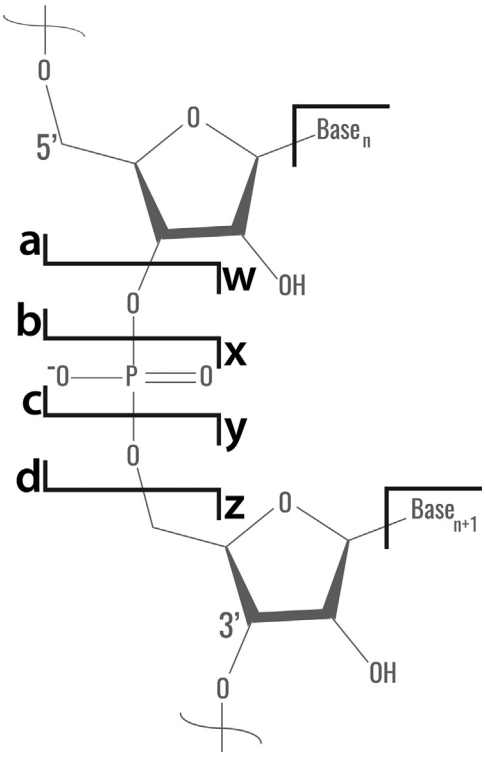


FIG. 1. **Nomenclature of nucleic acid fragmentation.**

## RESULTS AND DISCUSSION

### *Dissociation of PS-modified RNAs*

To elucidate the impact of PS modifications on MS/MS dissociation, we generated a library of variably modified PS RNAs. For a 20 nucleotide RNA sequence, a version with 19 phosphate linkages (unmodified RNA) and a version with 19 PS linkages (Fullps RNA) were created. To test the site-specific dependence of this modification, as well as the ability of electron- and collision-based activation methods to localize PS modifications, we generated 11 versions of the 20-mer RNA with variable PS incorporation rates. We assessed the performance of each activation method using sequence coverage, total matched fragment ions, and total base-loss fragment ions, using oligonucleotide fragmentation nomenclature pioneered by McLuckey *et al.* (23). We performed LC–MS on a mixture of 11 variations of the PS-modified 20-mer RNA on a hydrophilic interaction chromatography column, and the total ion chromatogram shows a clean separation between the elution of each siRNA peak (Fig. 2). As the number of PS modifications increase, the RNA elutes earlier in the gradient, with the Fullps RNA eluting the earliest and 9ps RNA eluting last among the 11 siRNAs studied here. This difference in elution time indicates that the PS backbone is more hydrophobic than the phosphate analog, consistent with sulfur being less electronegative than oxygen and preferring hydrophobic environments (15, 76).

First, we performed AI-NETD to analyze the unmodified and fully PS-modified RNAs. Figure 3 presents AI-NETD MS/MS for several variably modified PS RNAs. While the unmodified RNA gave entirely d- and w-type ions, as has been reported previously for similar RNAs, the Fullps RNA produced a-, a•-, z-, and z•-type ions in addition to standard d- and w-type ions (Fig. 3*B*). Among the variably modified PS RNAs, PS modifications were excluded starting from the nucleotide linkages on 3′ terminus and 5′ terminus ends of the molecule. The 18ps RNA has one less PS modification than the Fullps RNA, having a standard phosphodiester linkage between the last two nucleotides on the 3′ terminus rather than a PS linkage. Similarly, the 17ps RNA lacks a PS modification between the two nucleotides on the 3′ terminus and 5′ terminus, being replaced by phosphodiester bonds.

For 17ps , 18ps, and Fullps RNAs ($z$ = −10), the fragmentation spectra have similar profiles. Impressively, full sequence coverage was attained with AI-NETD for all RNAs studied here with 231, 204, and 264 matched fragment ions for the Fullps RNA, the 18ps RNA, and the 17ps RNA, respectively (Fig. 3*A*). The distribution of the fragment ions was consistent across all the modified RNAs: a-, a•-, z-, and z•-type ions comprised about 40% of the ions with the remaining 60% of signal being d- and w- type ions. The corresponding unmodified RNA lacked these characteristic a- and z-type ions (Fig. 3*B*), and over 99% of fragment ion intensity came from d- and w-type ions.

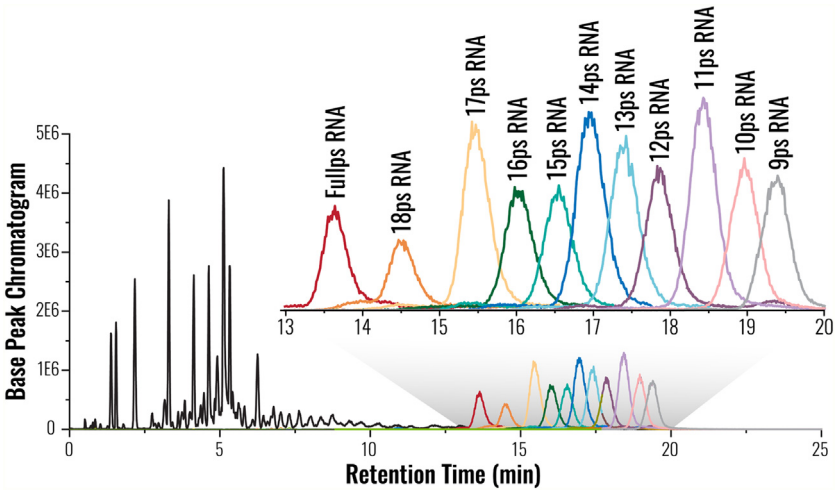


FIG. 2. **HILIC LC–MS base peak chromatogram reveals separation of 11 siRNAs used in this study, each with the same primary sequence but a variable degree of phosphorothioate linkages.** Extracted ion chromatograms for each RNA are each shown in a unique color. HILIC, hydrophilic interaction chromatography.

Annotated fragment ions and *m/z* values for two exemplary subsets of the AI-NETD spectra are shown in Figure 3, *C* and *D* to portray the similarity of ion intensity and distribution for the fragments. Between molecules, the same product ions were nearly always observed with mass differences of ±15.98 Da because of the variable number of substituted sulfur atoms (monoisotopic mass = 31.972 Da) for nonbridging oxygen atoms (monoisotopic mass = 15.995 Da) within these PS RNAs. Fragment masses are dependent on the location of PS modifications in relation to the dissociation site and allow for the site-specific localization of the modification. For example, in the Fullps RNA spectrum, the $w_7$ ion (*m/z* = 597.78, *z* = –4) includes the 3′-terminal PS modification between the last two nucleotides, whereas the same $w_7^{4-}$ ion in the 18ps RNA (*m/z* 593.53) lacks this PS modification. This difference in mass-to-charge ratio translates into a 15.98 Da shift, consistent with a sulfur substitution for an oxygen atom (Fig. 3*C*).

Mass shifts of the product ions in relation to the backbone dissociation sites are crucial to reveal the location of the PS modification. Among the variably modified PS RNAs, PS modifications were excluded starting from the nucleotide linkages on 3′ terminus and 5′ terminus ends of the molecule. The 18ps RNA has one less PS modification than the Fullps RNA, having a phosphodiester linkage between the last two nucleotides on the 3′ terminus rather than a PS linkage. Similarly, the 17ps RNA lacks a PS modification between the two nucleotides on the 3′ terminus and 5′ terminus, being replaced by phosphodiester bonds.

Because of the 17ps RNA missing a PS linkage from both terminal nucleotides, the spectra, on the other hand, have all matched a/b/c/d/w/x/y/z ions shifted by 15.98 Da from the Fullps RNA. The a/b/c/d ions have a mass shift as they include the 5′ terminus, which lacks a PS modification. Therefore, $w_7^{4-}$ ion has a mass shift to *m/z* 593.53, and the $a_2^{1-}$ ion has a 15.98 Da mass shift from *m/z* 570.09 to 554.10 (Fig. 3*C*). Although not depicted, note that a mass shift does not occur in a/b ions when the PS modification is at this backbone linkage. The same trend is seen in Figure 3*D* within the higher *m/z* range of 800 to 900 for all fragment ions: a 15.98 Da mass shift in w/x/y/z ions from Fullps RNA to 18ps RNA and an additional 15.98 Da mass shift in a/b/c/d ions from 18ps RNA to 17ps RNA. Comparing the Fullps RNA spectrum to the 17ps RNA spectrum, all matched ions a/b/c/d/w/x/y/z are shifted by 15.98 Da, the result of a PS modification on both terminal nucleotide linkages (Fig. 3, *C* and *D*).

### *PS impact on MS/MS dissociation*

The drastic difference between PS-modified RNA and unmodified RNA calls for an investigation into the spectra to understand the significance of these a- and z-type ions. We assessed the dissociation of the unmodified RNA and nine variably PS-modified RNA to compare the fragment-type composition at each bond cleavage site across each RNA. By incorporating one PS modification at a time, we could discern that a- and z-type ions were generated only at sites of PS linkages with AI-NETD (Fig. 4). Unmodified RNA is comprised of d- and w- type ions at all bond cleavage sites; bond cleavage at sites of PS incorporation is directed across d- and w- as well as a- and z- type ions. For the 9ps RNA with alternating phosphodiester and PS linkages, a-, d-, w-, and z-type type ions are detected only at PS sites and alternate with the d- and w-type ions at phosphodiester sites. As we approach a fully modified RNA, this trend continues, with AI-NETD of the Fullps RNA (19 PS modifications) producing a- and z-type ion at each bond cleavage site (Fig. 4).

Although a- and z-type ions are not the exclusive ions formed within the AI-NETD fragmentation landscape, their

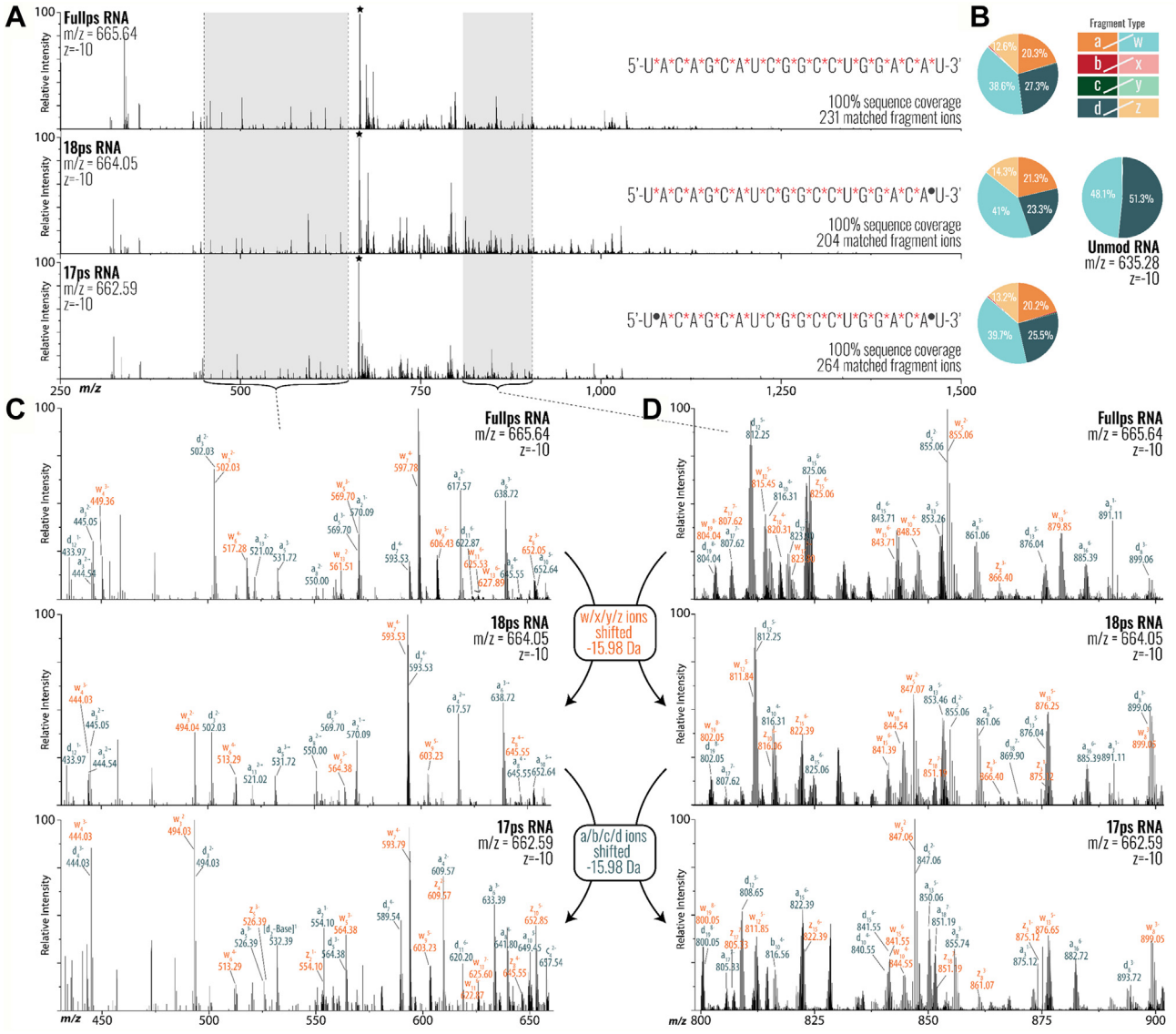


FIG. 3. **Comparison of AI-NETD tandem mass spectra depicting the site-specific detection of phosphorothioate (PS) incorporation.** *A*, AI-NETD spectra for the RNA with 19 PS linkages (Fullps RNA) and the RNAs with one and two unmodified phosphate linkages are shown, revealing similar fragmentation that translates to 100% sequence coverage and over 200 matched fragment ions for each of the $z = -10$ precursors. Peaks in the spectrum with a star denote remaining unreacted precursor. Within the RNA sequence, phosphate linkages are denoted by a *circle* (•), and PS linkages are denoted by an *asterisk* (*). *B*, fragmentation profiles for the three PS RNA as well as the unmodified reference RNA ($z = -10$). *C* and *D*, insets compare the indicated regions of the spectra, demonstrating that AI-NETD can site-specifically reveal the modification location, even when only the 5′-terminal residue or the 3′-terminal residue is unmodified. AI-NETD, activated ion electron transfer dissociation.

detection consistently and uniquely corresponds with site-specific PS modification. The bond cleavage sites 1 and 19 nucleotides from the 5′ terminus of Fullps RNA and 17ps RNA is dominated by d- and w-type fragment ions; however, the Fullps RNA has a discernible presence of a- and z-type ions at these cleavage positions (supplemental Figs. S1 and S2). The detection of a- and z-type ions is especially noteworthy as $d_{n-1}$ ions can be formed from $a_n$-type ions, whereas $w_{n-1}$ ions can be formed from $z_n$-type ions (35). Therefore, we hypothesize that not only does the sulfur substitution in the backbone direct initial electron transfer but also it allows for increased gas-phase stability of a- and z-type ions, accounting for their presence in modified fragmentation sites and the absence in unmodified fragmentation sites ("Ion stability offered by AI-NETD" section and Fig. 6).

As a point of comparison, we studied the effect of PS modifications on the dissociation of RNA in CAD and HCD MS/MS experiments and observed a change in distribution of product ions between unmodified and modified molecules. Although these methods generally produce c/y ion pairs, we

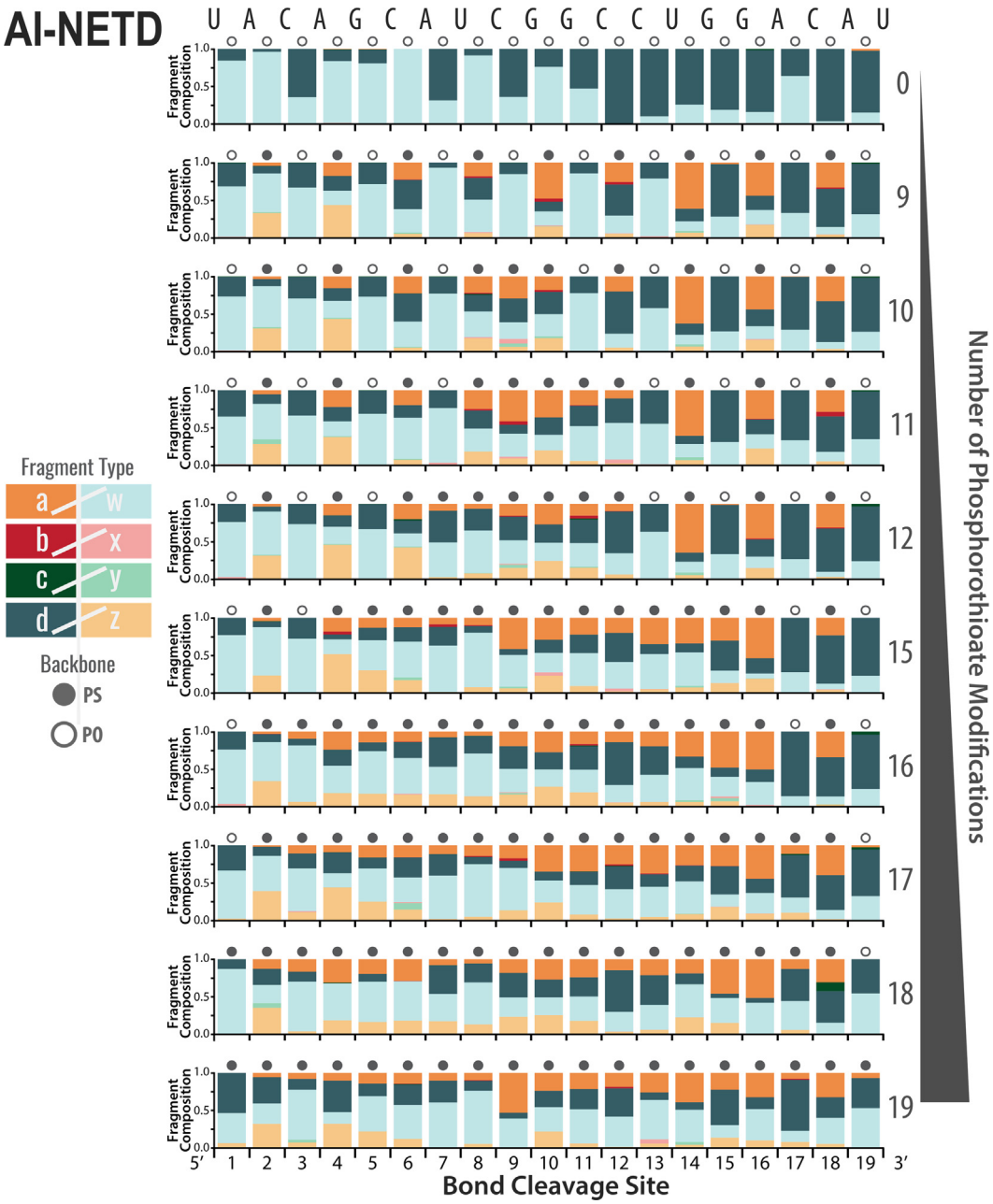


FIG. 4. **Site-specific mapping of RNA backbone modifications with AI-NETD.** Fragment composition of varying PS-modified RNA is depicted and arranged from least to most amount of PS modifications in the RNA. The *filled dot* and *open dot* above a bond cleavage site indicate a PS-modified and -unmodified backbone, respectively. Bond cleavage sites that have a PS modification have increased presence of a- and z-type ions compared with the same unmodified site, suggesting that PS modifications offer a- and z-type ion stability in the gas phase. AI-NETD, activated ion electron transfer dissociation; PS, phosphorothioate.

observe an increase in b/x ion pairs in RNA with more PS modifications. For HCD spectra, c- and y-type ions composed the majority of fragment ions (Fig. 5, *A–C*). However, as the number of PS modifications increase from 0 to 19, the intensity of complementary b- and x-type ions increases from 21.7% to 40% of the total annotated signal. Upon closer examination, we observe that incorporation of a single PS modification drives dissociation along b- and x- type ion channels at that residue, regardless of where in the sequence the PS is introduced (supplemental Fig. S3). A similar trend is observed for CAD spectra (supplemental Fig. S4). An increase in PS modifications is accompanied by an increase in b- and x- ion types from 22% to 38.6%, whereas c/y ions remain relatively stable as the predominant ion pair (Fig. 5*D*). The percentage of c/y ions remains relatively stable as the major ions, whereas b/x ions surpass other fragment ions as the

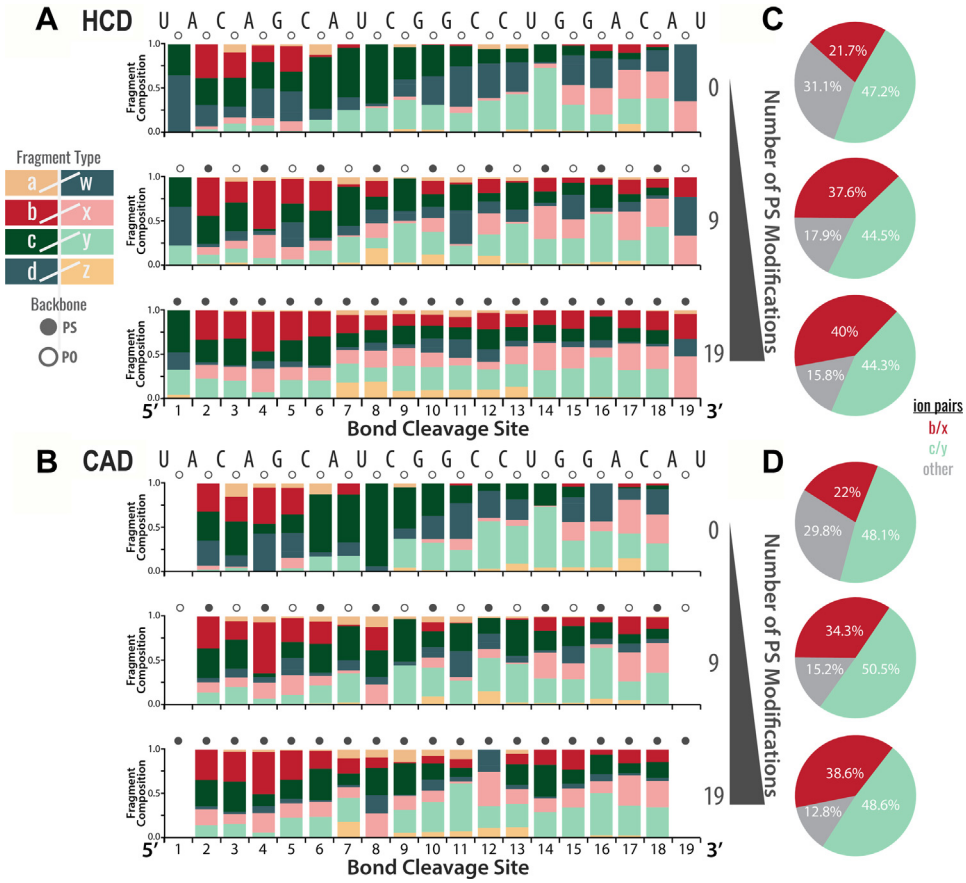


FIG. 5. **Site-specific mapping of RNA backbone modifications with collision-based HCD and CAD.** Fragment composition of RNA with varying amounts of PS modifications, arranged from least to the greatest number of modifications, for (*A*) HCD and (*B*) CAD fragmentation at the 19 possible cleavage sites. *Open and closed dots* above each bond cleavage site denote the absence and presence of PS modification in the backbone, respectively. Note that CAD lacks the 3′ and 5′ terminus fragment ions because of low mass cutoff in the ion trap. Fragmentation profiles of ion pairs for (*C*) HCD and (*D*) CAD fragmentation of the corresponding modified RNA on the *left*. CAD, collision-activated dissociation; HCD, higher-energy collisional dissociation; PS, phosphorothioate.

number of PS modifications increases (Fig. 5*D*). Despite these affected RNA dissociation channels during collision-based activation, the changes are not as discrete when compared with AI-NETD spectra. The dissociation of RNA with HCD and CAD yield b- and x- type ions at bond cleavage sites 2 through 5 (distance form 5′ terminus) regardless of modification status (Fig. 5, *A* and *B*). With AI-NETD, the presence of a- and z-type ions nearly always indicates the presence of a PS modification at that bond cleavage site (and vice versa). In addition, AI-NETD fragmentation produces fewer base loss compared with HCD and CAD (supplemenatal Figs. S5 and S6), producing a less convoluted spectra, which is easier to interpret. For the fully PS-modified RNA, a-, d-, w-, and z-type ions appear in roughly equal intensities.

### *Ion stability offered by AI-NETD*

As $d_{n-1}$ ions can be formed from $a_n$-type ions, and $w_{n-1}$ ions can be formed from $z_n$-type ions (35), we hypothesize that the sulfur allows for increased gas-phase stability of a- and z-type ions. To illustrate the hypothesis that PS modifications impact RNA dissociation channels, the dissociation pathway of RNA with a reagent cation is depicted in Figure 6. As the radical migrates onto the RNA backbone and causes an initial cleavage at site n, complementary $d_n\bullet/z_n$-type ions or $a_n/w_n\bullet$-type ions are formed. The $z_n$-type ion can undergo a hydrogen atom migration from the 2′-carbon to the 3′-phosphate or thiol, yielding a $w_{n-1}\bullet$ ion (Fig. 6). In a similar fashion, the $a_n$-type ion can dissociate into a $d_{n-1}\bullet$ ion (Fig. 6). This resulting d- and w-type ion pair accounts for the commonly seen dissociation pattern of unmodified RNA with electron-based MS/MS. The addition of PS modifications to RNA showed consistent presence of a- and z-type ions at modified backbone locations, encouraging the conclusion that the sulfur offers greater stability to these ions and limits dissociation into d•- and w•-type ions.

This stability in PS can be explained by the bond strength difference between X-H, where X is either an oxygen or a sulfur, and the gas-phase acidity of phosphate *versus* PS (77, 78). A free radical on oxygen abstracting a hydrogen from S-H, with a lower bond dissociation energy, forms an O-H bond,

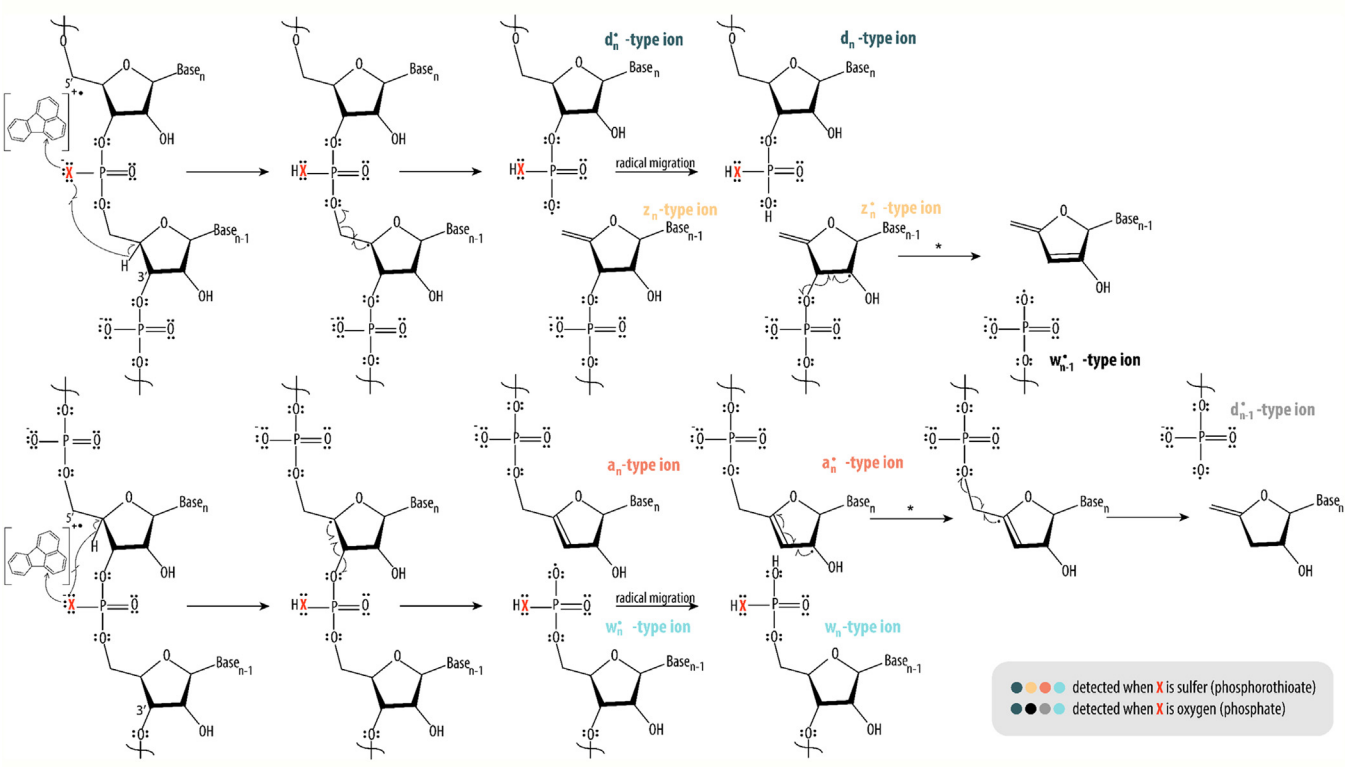


FIG. 6. **Proposed scheme of phosphorothioate RNA dissociation with AI-NETD.** *Top*, dissociation pathway into complementary d- and z-type ions with radical migration producing w-type ions. *Bottom*, dissociation pathway into complementary a- and w-type ions with radical migration producing d-type ions. AI-NETD, activated ion electron transfer dissociation.

with higher X-H bond dissociation energy and stability (79). Correspondingly, the free radical on sulfur offers more stability than that of an oxygen and hinders the free radical from transferring to the complementary fragment ion for further dissociation. As a result, the a- and z-type ions are preserved and appear in higher abundance in RNA with PS modifications. Furthermore, several groups have shown that IR photoactivation unfolds peptide cations to limit hydrogen atom migration events (68, 80–82). We conclude that PS offers gas-phase stability to the radical fragments.

## CONCLUSION

Modifications on RNAs confer properties crucial for therapeutic approaches, and quality assessments of these synthesized RNA are important in determining impurities that may be present. Here, we demonstrate the utility of AI-NETD in diagnosing site-specific PS incorporation with complete sequence coverage of every molecule studied while producing fewer base-loss fragment ions than collision-based methods. In addition, our work reveals the gas-phase stability that PS imparts on RNA dissociation mechanisms.

With the addition of PS modifications to RNA, dissociation channels change for electron-based and collision-based methods. While an increase in b- and x-type ion production was observed with collision-based methods, an increase of a- and z-type ions was observed for AI-NETD more consistently at PS linkages, and AI-NETD serves more as a diagnostic tool in identifying the presence of PS modifications in an RNA. Fewer base-loss fragments were produced with AI-NETD than HCD and CAD, allowing for a cleaner spectrum for interpretation.

Investigating the diagnostic a- and z-type ions from AI-NETD dissociation led to the conclusion that PS linkages offer gas-phase stability to radical fragment ions. Hydrogen abstraction from a thiol by a radical oxygen results in a more stabilizing bond with hydrogen and radical sulfur. With sulfur bearing the radical, radical migration is hindered, and a- and z-type ions are better preserved and detected by the mass spectrometer. This alteration of PS RNA dissociation prompts inclusion of a- and z-type product ions beyond the standard d- and w-type ions for electron-based oligonucleotide MS/MS for modified RNA. Furthermore, HCD and CAD spectra of intact or digested RNA typically reveal c- and y-type product ions; however, PS incorporation drives site-specific production of complementary b- and x-type ions in near equal proportion to standard c- and y-type ions.

## DATA AVAILABILITY

Raw data files are available online on Chorus (Project ID: 1789).

*Supplemental data*—This article contains supplemental data.

*Acknowledgments*—We thank John E. P. Syka, Josh Hinkle, James L. Stephenson, and other members of the Coon Laboratory for helpful discussions.

*Funding and additional information*—This work was supported by the National Institute of General Medical Sciences of the National Institutes of Health (grant no.: P41GM108538; to J. J. C.) and the National Human Genome Research Institution through a training grant to the Genomic Science Training Program (grant no.:T32HG002760; to T. M. P.-C.). T. M. P.-C. acknowledges the ACS Division of Analytical Chemistry and Agilent for support through a graduate fellowship. B. J. A. acknowledges support from NLM Computation and Informatics in Biology and Medicine training grant 5T15LM007359.

*Author contributions*—T. M. P.-C., W. M. M., and J. J. C. conceptualization; T. M. P.-C. and W. M. M. methodology; T. M. P.-C. and Q. Q. software; T. M. P.-C., B. J. A., W. M. M., E. L., M. S. W., and J. J. C. validation; T. M. P. C. formal analysis; T. M. P.-C. and Q. Q. writing–original draft; T. M. P.-C., Q. Q., and J. J. C. writing–review & editing; T. M. P.-C. and B. J. A. visualization; J. J. C. visualization; J. J. C. funding acquisition.

*Conflict of interest*—J. J. C. is a consultant for Thermo Fisher Scientific, 908 Devices, and Seer. All other authors declare no competing interests.

*Abbreviations*—The abbreviations used are: AI-NETD, activated ion NETD; CAD, collision-activated dissociation; ETD, electron transfer dissociation; gRNA, guide RNA; HCD, higher-energy collisional dissociation; MPB, mobile phase B; MS, mass spectrometry; NETD, negative electron transfer dissociation; PS, phosphorothioate.

Received December 19, 2023 Published, MCPRO Papers in Press, February 23, 2024, https://doi.org/10.1016/j.mcpro.2024.100742

REFERENCES

1. Coon, J. J., Shabanowitz, J., Hunt, D. F., and Syka, J. E. P. (2005) Electron transfer dissociation of peptide anions. *J. Am. Soc. Mass Spectrom.* **16**, 880–882
2. Zamecnik, P. C., and Stephenson, M. L. (1978) Inhibition of rous sarcoma virus replication and cell transformation by a specific oligodeoxynucleotide. *Proc. Natl. Acad. Sci. U. S. A.* **75**, 280–284
3. Stephenson, M. L., and Zamecnik, P. C. (1978) Inhibition of rous sarcoma viral RNA translation by a specific oligodeoxyribonucleotide. *Proc. Natl. Acad. Sci. U. S. A.* **75**, 285–288
4. Bennett, C. F., and Swayze, E. E. (2010) RNA targeting therapeutics: molecular mechanisms of antisense oligonucleotides as a therapeutic platform. *Annu. Rev. Pharmacol. Toxicol.* **50**, 259–293
5. Kole, R., Krainer, A. R., and Altman, S. (2012) RNA therapeutics: beyond RNA interference and antisense oligonucleotides. *Nat. Rev. Drug Discov.* **11**, 125–140
6. Chernikov, I. V., Vlassov, V. V., and Chernolovskaya, E. L. (2019) Current development of SiRNA bioconjugates: from research to the clinic. *Front. Pharmacol.* **10**, 444
7. Karikó, K., Muramatsu, H., Welsh, F. A., Ludwig, J., Kato, H., Akira, S., *et al*. (2008) Incorporation of pseudouridine into MRNA yields superior nonimmunogenic vector with increased translational capacity and biological stability. *Mol. Ther.* **16**, 1833–1840
8. Andries, O., Mc Cafferty, S., De Smedt, S. C., Weiss, R., Sanders, N. N., and Kitada, T. (2015) N1-methylpseudouridine-incorporated MRNA outperforms pseudouridine-incorporated MRNA by providing enhanced protein expression and reduced immunogenicity in mammalian cell lines and mice. *J. Control. Release* **217**, 337–344
9. Anderson, B. R., Muramatsu, H., Nallagatla, S. R., Bevilacqua, P. C., Sansing, L. H., Weissman, D., *et al*. (2010) Incorporation of pseudouridine into MRNA enhances translation by diminishing PKR activation. *Nucleic Acids Res.* **38**, 5884–5892
10. Nance, K. D., and Meier, J. L. (2021) Modifications in an emergency: the role of N1-methylpseudouridine in COVID-19 vaccines. *ACS Cent. Sci.* **7**, 748–756
11. Corbett, K. S., Edwards, D. K., Leist, S. R., Abiona, O. M., Boyoglu-Barnum, S., Gillespie, R. A., *et al*. (2020) SARS-CoV-2 MRNA vaccine design enabled by prototype pathogen preparedness. *Nature* **586**, 567–571
12. Joffe, S. (2021) Evaluating SARS-CoV-2 vaccines after emergency use authorization or licensing of initial candidate vaccines. *JAMA* **325**, 221–222
13. Levin, A. A. A. (1999) Review of issues in the pharmacokinetics and toxicology of phosphorothioate antisense oligonucleotides. *Biochim. Biophys. Acta* **1489**, 69–84
14. Eckstein, F. (2000) Phosphorothioate oligodeoxynucleotides: what is their origin and what is unique about them? *Antisense Nucleic Acid Drug Dev.* **10**, 117–121
15. Eckstein, F. (2014) Phosphorothioates, essential components of therapeutic oligonucleotides. *Nucleic Acid Ther.* **24**, 374–387
16. Schurch, S., Bernal-Mendez, E., and Leumann, C. J. (2002) Electrospray tandem mass spectrometry of mixed-sequence RNA/DNA oligonucleotides. *J. Am. Soc. Mass Spectrom.* **13**, 936–945
17. Zhou, W., and Agrawal, S. (1998) Mixed-backbone oligonucleotides as second-generation antisense agents with reduced phosphorothioate-related side effects. *Bioorg. Med. Chem. Lett.* **8**, 3269–3274
18. Guga, P., Boczkowska, M., Janicka, M., Maciaszek, A., Nawrot, B., Antoszczyk, S., *et al*. (2006) Enhanced P-stereodependent stability of complexes formed by phosphorothioate oligonucleotides due to involvement of sulfur as strong hydrogen bond acceptor. *Pure Appl. Chem.* **78**, 993–1002
19. Santos, I. C., and Brodbelt, J. S. (2021) Recent developments in the characterization of nucleic acids by liquid chromatography, capillary electrophoresis, ion mobility, and mass spectrometry (2010–2020). *J. Sep. Sci.* **44**, 340–372
20. Schürch, S. (2016) Characterization of nucleic acids by tandem mass spectrometry - the second decade (2004 - 2013): from DNA to RNA and modified sequences. *Mass Spectrom. Rev.* **35**, 483–523
21. Largy, E., König, A., Ghosh, A., Ghosh, D., Benabou, S., Rosu, F., *et al*. (2022) Mass spectrometry of nucleic acid noncovalent complexes. *Chem. Rev.* **122**, 7720–7839
22. [preprint] Peters-Clarke, T. M., Coon, J. J., and Riley, N. M. (2023) Instrumentation at the Leading Edge of Proteomics. *chemRxiv*. https://doi.org/10.26434/chemrxiv-2023-8l72m
23. Mcluckey, S. A., Van Berkel, G. J., and Glish, G. L. (1992) Tandem mass spectrometry of small, multiply charged oligonucleotides. *J. Am. Soc. Mass Spectrom.* **3**, 60–70
24. Rodgers, M. T., Campbell, S., Marzluff, E. M., and Beauchamp, J. L. (1994) Low-energy collision-induced dissociation of deprotonated dinucleotides: determination of the energetically favored dissociation pathways and the relative acidities of the nucleic acid bases. *Int. J. Mass Spectrom. Ion Process.* **137**, 121–149
25. Taucher, M., Rieder, U., and Breuker, K. (2010) Minimizing base loss and internal fragmentation in collisionally activated dissociation of multiply deprotonated RNA. *J. Am. Soc. Mass Spectrom.* **21**, 278–285
26. Huang, T. Y., Liu, J., Liang, X., Hodges, B. D. M., and McLuckey, S. A. (2008) Collision-induced dissociation of intact duplex and single-stranded SiRNA anions. *Anal. Chem.* **80**, 8501–8508

27. Huang, T. Y., Kharlamova, A., Liu, J., and McLuckey, S. A. (2008) Ion trap collision-induced dissociation of multiply deprotonated RNA: c/y-Ions versus (a-B)/w-Ions. *J. Am. Soc. Mass Spectrom.* **19**, 1832–1840
28. [preprint] Sun, R., Zuo, M., Zhang, J., and Dong, M. (2023) Charge-state-dependent collision-induced dissociation behaviors of RNA oligonucleotides via high-resolution mass spectrometry. *bioRxiv*. https://doi.org/10.1101/2023.01.29.526146
29. Wah, T., Chan, D., Choy, M. F., Yi, W., Chan, K., Man, Y., *et al*. (2011) A mechanistic study of the electron capture dissociation of oligonucleotides. *J. Am. Soc. Mass Spectrom.* **20**, 213–226
30. Schultz, K. N., and Håkansson, K. (2004) Rapid electron capture dissociation of mass-selectively accumulated oligodeoxynucleotide dications. *Int. J. Mass Spectrom.* **234**, 123–130
31. Håkansson, K., Hudgins, R. R., Marshall, A. G., and O'Hair, R. A. (2003) J. Electron capture dissociation and infrared multiphoton dissociation of oligodeoxynucleotide dications. *J. Am. Soc. Mass Spectrom.* **14**, 23–41
32. Smith, S. I., and Brodbelt, J. S. (2009) Electron transfer dissociation of oligonucleotide cations. *Int. J. Mass Spectrom.* **283**, 85–93
33. Hari, Y., Leumann, C. J., and Schürch, S. (2017) What hinders electron transfer dissociation (ETD) of DNA cations? *J. Am. Soc. Mass Spectrom.* **28**, 2677–2685
34. Huang, T. Y., and McLuckey, S. A. (2011) Gas-phase ion/ion reactions of rubrene cations and multiply charged DNA and RNA anions. *Int. J. Mass Spectrom.* **304**, 140–147
35. Gao, Y., and McLuckey, S. A. (2013) Electron transfer followed by collision-induced dissociation (NET-CID) for generating sequence information from backbone-modified oligonucleotide anions. *Rapid Commun. Mass Spectrom.* **27**, 249–257
36. Gao, Y., Yang, J., Cancilla, M. T., Meng, F., and McLuckey, S. A. (2013) Top-down interrogation of chemically modified oligonucleotides by negative electron transfer and collision induced dissociation. *Anal. Chem.* **85**, 4713–4720
37. McLuckey, S. A., Wu, J., Bundy, J. L., Stephenson, J. L., and Hurst, G. B. (2002) Oligonucleotide mixture analysis via electrospray and ion/ion reactions in a quadrupole ion trap. *Anal Chem.* **74**, 976–984
38. Peters-Clarke, T. M., Quan, Q., Brademan, D. R., Hebert, A. S., Westphall, M. S., and Coon, J. J. (2020) Ribonucleic acid sequence characterization by negative electron transfer dissociation mass spectrometry. *Anal Chem.* **92**, 4436–4444
39. Herron, W. J., Goeringer, D. E., and McLuckey, S. A. (1995) Gas-phase electron transfer reactions from multiply-charged anions to rare gas cations. *J. Am. Chem. Soc.* **117**, 11555–11562
40. Stephenson, J. L., and McLuckey, S. A. (1997) Charge reduction of oligonucleotide anions via gas-phase electron transfer to xenon cations. *Rapid Commun. Mass Spectrom.* **11**, 875–880
41. McLuckey, S. A., Stephenson, J. L., and O'Hair, R. A. (1997) J. Decompositions of odd- and even-electron anions derived from deoxypolyadenylates. *J. Am. Soc. Mass Spectrom.* **8**, 148–154
42. Yang, J., and Håkansson, K. (2006) Fragmentation of oligoribonucleotides from gas-phase ion-electron reactions. *J. Am. Soc. Mass Spectrom.* **17**, 1369–1375
43. Taucher, M., and Breuker, K. (2010) Top-down mass spectrometry for sequencing of larger (up to 61 Nt) RNA by CAD and EDD. *J. Am. Soc. Mass Spectrom.* **21**, 918–929
44. Taucher, M., and Breuker, K. (2012) Characterization of modified RNA by top-down mass spectrometry. *Angew. Chem.* **51**, 11289–11292
45. Ausgabe, D., Calderisi, G., Glasner, H., and Breuker, K. (2020) Radical transfer dissociation for de novo characterization of modified ribonucleic acids by mass spectrometry. *Angew. Chem.* **132**, 4339–4343
46. Smith, S. I., and Brodbelt, J. S. (2011) Hybrid activation methods for elucidating nucleic acid modifications. *Anal. Biochem.* **83**, 303–310
47. Santos, I. C., Lanzillotti, M., Shilov, I., Basanta-Sanchez, M., Roushan, A., Lawler, R., *et al*. (2022) Ultraviolet photodissociation and activated electron photodetachment mass spectrometry for top-down sequencing of modified oligoribonucleotides. *J. Am. Soc. Mass Spectrom.* **33**, 510–520
48. Gabelica, V., Tabarin, T., Antoine, R., Compagnon, I., Broyer, M., De Pauw, E., *et al*. (2006) Electron photodetachment dissociation of DNA polyanions in a quadrupole ion trap mass spectrometer. *Anal Chem.* **78**, 6564–6572
49. Cannon, J. R., Holden, D. D., and Brodbelt, J. S. (2014) Hybridizing ultraviolet photodissociation with electron transfer dissociation for intact protein characterization. *Anal. Chem.* **86**, 10970–10977
50. Shaw, J. B., Madsen, J. A., Xu, H., and Brodbelt, J. S. (2012) Systematic comparison of ultraviolet photodissociation and electron transfer dissociation for peptide anion characterization. *J. Am. Chem. Soc.* **23**, 1707–1715
51. Gabelica, V., Rosu, F., Tabarin, T., Kinet, C., Antoine, R., Broyer, M., *et al*. (2007) Base-dependent electron photodetachment from negatively charged DNA strands upon 260-Nm laser irradiation. *J. Am. Chem. Soc.* **129**, 4706–4713
52. Smith, S. I., and Brodbelt, J. S. (2010) Characterization of oligodeoxynucleotides and modifications by 193 Nm photodissociation and electron photodetachment dissociation. *Anal Chem.* **82**, 7218–7226
53. Goyon, A., Scott, B., Kurita, K., Maschinot, C., Meyer, K., Yehl, P., *et al*. (2022) On-line sequencing of CRISPR guide RNAs and their impurities via the use of immobilized ribonuclease cartridges attached to a 2D/3D-LC–MS system. *Anal Chem.* **94**, 1169–1177
54. Goyon, A., Scott, B., Kurita, K., Crittenden, C. M., Shaw, D., Lin, A., *et al*. (2021) Full sequencing of CRISPR/Cas9 single guide RNA (SgRNA) via parallel ribonuclease digestions and hydrophilic interaction liquid chromatography-high-resolution mass spectrometry analysis. *Anal Chem.* **93**, 14792–14801
55. Gaston, K. W., and Limbach, P. A. (2015) The identification and characterization of non-coding and coding RNAs and their modified nucleosides by mass spectrometry. *RNA Biol.* **11**, 1568–1585
56. Wolf, E. J., Grünberg, S., Grünberg, G., Dai, N., Chen, T.-H., Roy, B., *et al*. (2013) Human RNase 4 improves MRNA sequence characterization by LC–MS/MS. *Nucleic Acids Res.* **1**, 13–14
57. Vanhinsbergh, C. J., Criscuolo, A., Sutton, J. N., Murphy, K., Williamson, A. J. K., Cook, K., *et al*. (2022) Characterization and sequence mapping of large RNA and MRNA therapeutics using mass spectrometry. *Anal Chem.* **94**, 7339–7349
58. Pimentel, E., Peters-Clarke, T., Coon, J., and Martell, J. (2021) DNA-scaffolded synergistic catalysis. *J. Am. Chem. Soc.* **143**, 21402–21409
59. Crittenden, C. M., Lanzillotti, M. B., and Chen, B. (2023) Top-down mass spectrometry of synthetic single guide ribonucleic acids enabled by facile sample clean-up. *Anal Chem.* **95**, 3180–3186
60. Merrifield, J. L., Pimentel, E. B., Peters-Clarke, T. M., Nesbitt, D. J., Coon, J. J., and Martell, J. D. (2023) DNA-compatible copper/TEMPO oxidation for DNA-encoded libraries. *Bioconjug. Chem.* **34**, 1380–1386
61. Riley, N. M., Rush, M. J. P., Rose, C. M., Richards, A. L., Kwiecien, N. W., Bailey, D. J., *et al*. (2015) The negative mode proteome with activated ion negative electron transfer dissociation (AI-NETD). *Mol. Cell Proteomics* **14**, 2644–2660
62. Rush, M. J. P., Riley, N. M., Westphall, M. S., Syka, J. E. P., and Coon, J. J. (2017) Sulfur pentafluoride is a preferred reagent cation for negative electron transfer dissociation. *J. Am. Soc. Mass Spectrom.* **28**, 1324–1332
63. McAlister, G. C., Russell, J. D., Rumachik, N. G., Hebert, A. S., Syka, J. E. P., Geer, L. Y., *et al*. (2012) Analysis of the acidic proteome with negative electron-transfer dissociation mass spectrometry. *Anal Chem.* **84**, 2875–2882
64. Rumachik, N. G., McAlister, G. C., Russell, J. D., Bailey, D. J., Wenger, C. D., and Coon, J. J. (2012) Characterizing peptide neutral losses induced by negative electron-transfer dissociation (NETD). *J. Am. Soc. Mass Spectrom.* **23**, 718–727
65. Riley, N. M., Bern, M., Westphall, M. S., and Coon, J. J. (2016) Full-featured search algorithm for negative electron-transfer dissociation. *J. Proteome Res.* **15**, 2768–2776
66. Syka, J. E. P., Coon, J. J., Schroeder, M. J., Shabanowitz, J., and Hunt, D. F. (2004) Peptide and protein sequence analysis by electron transfer dissociation mass spectrometry. *Proc. Natl. Acad. Sci. U. S. A.* **101**, 9528–9533
67. Zubarev, R. A., Kelleher, N. L., McLafferty, F. W., and October, R. V. (1998) Electron capture dissociation of multiply charged protein cations. A nonergodic process. *J. Am. Chem. Soc.* **120**, 3265–3266
68. Peters-Clarke, T., Riley, N., Westphall, M. S., and Coon, J. (2022) Practical effects of intramolecular hydrogen rearrangement in electron transfer dissociation-based proteomics. *J. Am. Soc. Mass Spectrom.* **33**, 100–110

69. Peters-Clarke, T., Schauer, K., Riley, N., Lodge, J., Westphall, M., and Coon, J. (2020) Optical fiber-enabled photoactivation of peptides and proteins. *Anal Chem.* **92**, 12363–12370
70. Riley, N. M., Westphall, M. S., Hebert, A. S., and Coon, J. J. (2017) Implementation of activated ion electron transfer dissociation on a quadrupole-orbitrap-linear ion trap hybrid mass spectrometer. *Anal Chem.* **89**, 6358–6366
71. Carell, T., Brandmayr, C., Hienzsch, A., Müller, M., Pearson, D., Reiter, V., *et al*. (2012) Structure and function of noncanonical nucleobases. *Angew. Chem. Int. Ed. Engl.* **51**, 7110–7131
72. Cantara, W. A., Crain, P. F., Rozenski, J., McCloskey, J. A., Harris, K. A., Zhang, X., *et al*. (2011) The RNA modification database, RNAMDB: 2011 update. *Nucleic Acids Res.* **39**(suppl_1), D195–D201
73. Machnicka, M. A., Milanowska, K., Oglou, O. O., Purta, E., Kurkowska, M., Olchowik, A., *et al*. (2013) MODOMICS: a database of RNA modification pathways—2013 update. *Nucleic Acids Res.* **41**, D262–D267
74. Boccaletto, P., MacHnicka, M. A., Purta, E., Pitkowski, P., Baginski, B., Wirecki, T. K., *et al*. (2018) MODOMICS: a database of RNA modification pathways. 2017 update. *Nucleic Acids Res.* **46**, D303–D307
75. Boccaletto, P., Stefaniak, F., Ray, A., Cappannini, A., Mukherjee, S., Purta, E., *et al*. (2022) MODOMICS: a database of RNA modification pathways. 2021 update. *Nucleic Acids Res.* **50**, D231–D235
76. Eckstein, F. (1966) Nucleoside phosphorothioates. *J. Am. Chem. Soc.* **88**, 4292–4294
77. Thaplyal, P., and Bevilacqua, P. C. (2014) Experimental approaches for measuring PKa's in RNA and DNA. *Methods Enzymol.* **549**, 189–219
78. Remko, M., Liedl, K. R., and Rode, B. M. (1996) Gas-phase acidities of HM(=X) XH (M = C, Si; X = O, S) acids calculated by Ab initio molecular orbital methods at the G2 level of theory. *Chem. Phys. Lett.* **263**, 379–384
79. Dénès, F., Pichowicz, M., Povie, G., and Renaud, P. (2014) Thiyl radicals in organic synthesis. *Chem. Rev.* **114**, 2587–2693
80. Savitski, M. M., Kjeldsen, F., Nielsen, M. L., and Zubarev, R. A. (2007) Hydrogen rearrangement to and from radical z fragments in electron capture dissociation of peptides. *J. Am. Soc. Mass Spectrom.* **18**, 113–120
81. Rand, K. D., Adams, C. M., Zubarev, R. A., and Jørgensen, T. J. D. (2008) Electron capture dissociation proceeds with a low degree of intramolecular migration of peptide Amide hydrogens. *J. Am. Chem. Soc.* **130**, 1341–1349
82. Ledvina, A. R., McAlister, G. C., Gardner, M. W., Smith, S. I., Madsen, J. A., Schwartz, J. C., *et al*. (2009) Infrared photoactivation reduces peptide folding and hydrogen- atom migration following ETD tandem mass spectrometry. *Angew. Chem. Int. Ed. Engl.* **48**, 8526–8528